

Sigma : Siamese Mamba Network for Multi-Modal Semantic Segmentation

Zifu Wan¹ Yuhao Wang² Silong Yong¹ Pingping Zhang²
Simon Stepputtis¹ Katia Sycara¹ Yaqi Xie¹

¹ Robotics Institute, Carnegie Mellon University, USA

² School of Future Technology, Dalian University of Technology, China
{zifuw, silongy, sstepput, katia, yaqix}@andrew.cmu.edu,
yuhaoawangdlut@gmail.com, zhpp@dlut.edu.cn

Abstract. Multi-modal semantic segmentation significantly enhances AI agents’ perception and scene understanding, especially under adverse conditions like low-light or overexposed environments. Leveraging additional modalities (*X-modality*) like thermal and depth alongside traditional RGB provides complementary information, enabling more robust and reliable segmentation. In this work, we introduce Sigma, a Siamese Mamba network for multi-modal semantic segmentation, utilizing the Selective Structured State Space Model, Mamba. Unlike conventional methods that rely on CNNs, with their limited local receptive fields, or Vision Transformers (ViTs), which offer global receptive fields at the cost of quadratic complexity, our model achieves global receptive fields coverage with linear complexity. By employing a Siamese encoder and innovating a Mamba fusion mechanism, we effectively select essential information from different modalities. A decoder is then developed to enhance the channel-wise modeling ability of the model. Our method, Sigma, is rigorously evaluated on both RGB-Thermal and RGB-Depth segmentation tasks, demonstrating its superiority and marking the first successful application of State Space Models (SSMs) in multi-modal perception tasks. Code is available at <https://github.com/zifuwan/Sigma>.

Keywords: Multi-Modal Scene Understanding · Semantic Segmentation · State Space Model · Vision Mamba

1 Introduction

Semantic segmentation, aiming to assign a semantic label for each pixel within an image, has been increasingly significant for AI agents to accurately perceive their environment [4, 20]. However, current vision models still struggle in challenging conditions like low light or obstructive elements such as sun glare and fire [4, 71, 72]. With the goal of enhancing segmentation under such challenging conditions, additional modalities like thermal and depth are beneficial to enhance vision system robustness. With the supplementary information, the robustness

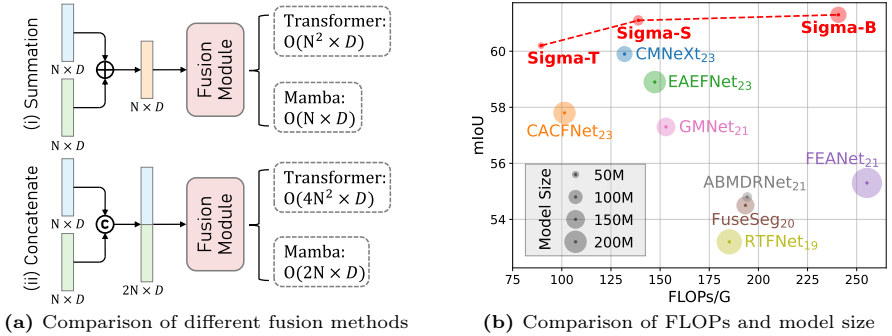



Fig. 1: (a) Comparative analysis of complexity across different fusion methods utilizing Transformer and Mamba: Mamba-based fusion approaches significantly reduce complexity by an order of magnitude compared to their Transformer-based counterparts. (b) Computation and model size comparison of Sigma and other methods. The size of each circle indicates the model size (parameters).

and capabilities of vision pipelines can be improved [30, 37, 73]. However, utilizing multiple modalities introduces additional challenges, namely the alignment and fusion of the information provided through these additional channels [12].

Previous approaches in multi-modal semantic segmentation rely on Convolutional Neural Networks (CNN) or Vision Transformers (ViT). While CNN-based approaches [13, 29] are known for their scalability and linear complexity, they suffer from the small receptive field limited by the kernel size, leading to local reductive bias. Besides, CNNs utilize a weight-sharing kernel across different parts of the input, limiting its flexibility in adapting to unseen or low-quality images. In contrast, ViT-based methods [1, 30, 52] offer enhanced visual modeling by leveraging global receptive fields and dynamic weights. However, their self-attention mechanism leads to quadratic complexity in terms of input sizes [16], raising efficiency concerns. Attempts to improve this efficiency by reducing the dimensions or stride of the processing windows compromise the extent of the receptive fields [66].

To address these limitations, Selective Structured State Space Models – Mamba [16] – have gained more popularity due to their global receptive field coverage and dynamic weights with linear complexity. Mamba has shown outstanding effectiveness in tasks involving long sequence modeling, notably in natural language processing [16]. Furthermore, more studies have explored its potential for vision-related applications, such as image classification [33], medical image segmentation [38, 41, 56, 60, 65], and 3D scene comprehension [28]. Inspired by these benefits, we introduce **Sigma** , a Siamese Mamba network for multi-modal sensor fusion utilizing the recent advances of Mamba and apply it to the challenging domain of semantic segmentation.

As depicted in Fig. 2, our Sigma integrates a Siamese encoder [63] for feature extraction, fusion modules for aggregating information from different modalities, and a decoder that is adapted to both spatial and channel-specific information. The encoder backbone utilizes cascaded *Visual State Space (VSS) Blocks* with

downsampling to extract multi-scale global information from various modalities. Subsequently, the extracted features are directed to a fusion module at each level, where multi-modal features initially interact through a *Cross Mamba Block (CroMB)* to augment cross-modal information. Following this, the enhanced features are processed by a *Concat Mamba Block (ConMB)*, which employs an attention mechanism to select pertinent information from each modality. Our fusion mechanism leverages the linear scaling property of Mamba, significantly reducing computational demand, as illustrated in Fig. 1a. Finally, the fused features are sent to multi-level *Channel-Aware Visual State Space (CVSS) Blocks* to effectively capture multi-scale long-range information.

We conduct comprehensive experiments on both RGB-Thermal [21, 45] and RGB-Depth datasets [46, 48], demonstrating that Sigma outperforms state-of-the-art models on both accuracy and efficiency, as depicted in Fig. 1b. Detailed ablation studies further validate the contribution of each component within Sigma to the overall model efficacy.

Our contributions can be summarized as follows:

- To our best knowledge, this marks the first successful application of State Space Models, specifically Mamba, in multi-modal semantic segmentation.
- We introduce an attention-based Mamba fusion mechanism alongside a channel-aware Mamba decoder, to efficiently extract information across different modalities and integrate them seamlessly.
- Comprehensive evaluations in RGB-Thermal and RGB-Depth domains showcase our method’s superior accuracy and efficiency, setting a new benchmark for future investigations into Mamba’s potential in multi-modal learning.

2 Related Work

2.1 Multi-Modal Semantic Segmentation

Multi-modal semantic understanding typically incorporates an RGB modality for widespread application, alongside other complementary modalities such as thermal, depth, LiDAR, *etc.* [12, 75]. These supplementary sensors offer crucial information to the vision system across various scenarios. For instance, thermal sensors detect infrared radiation, enabling the identification of targets in dark and foggy conditions through temperature differences. This capability is essential for applications such as surveillance, wildfire rescue operations, and wildlife monitoring [14]. Meanwhile, depth sensors ascertain the distance between the sensor and objects in the environment, furnishing a three-dimensional representation of the scene. This technology is extensively utilized in autonomous vehicles for obstacle detection and scene understanding [11]. To optimize the utilization of these additional modalities, the development of effective feature extractors and fusion mechanisms has been of paramount importance.

In RGB-Thermal semantic segmentation, early attempts usually design an encoder-decoder architecture with shortcut connection [21, 45, 49, 50], dense connection [50, 61, 77], dilated convolutions [62, 76], knowledge distillation [13], *etc.*

To mitigate the lack of global context understanding ability of CNNs, many methods apply attention mechanism in the feature fusion stage [29, 50, 77]. With the growing popularity of Transformers, more methods have begun to leverage them for extracting long-range dependencies from RGB and thermal images. CMX [30] utilizes SegFormer [59] for feature extraction and introduces a rectification module along with a cross-attention module for the fusion of features. Based on CMX [30], CMNeXt [73] proposes a self-query hub to select informative features from various supplementary modalities. More recently, SegMiF [32] employs a cascading structure coupled with a hierarchical interactive attention mechanism, ensuring the precise mapping of crucial information across two modalities.

In the domain of RGB-Depth semantic segmentation, methodologies that have proven effective in RGB-Thermal segmentation have also demonstrated impressive performance, such as CMX [30], CMNeXt [73]. Meanwhile, recent developments in self-supervised pre-training have paved the way for its exploration in RGB-Depth perception. For instance, MultiMAE [1] employs a Masked Autoencoder [23] approach with pseudo labeling, ingesting tokens from various modalities and reconstructing the masked tokens. DFormer [51] integrates both RGB and Depth modalities within the pre-training architecture to learn transferable multi-modal representations.

Although the aforementioned Transformer-based methods have shown promising results in RGB-X semantic segmentation due to their global context modeling capabilities, the quadratic scaling nature of the self-attention mechanism in Transformers limits the length of input sequences. Consequently, most approaches have to consolidate multi-modal tokens ($\mathcal{F}_{\text{RGB}}, \mathcal{F}_{\text{T}} \in \mathbb{R}^{N \times D}$) into a single token ($\mathcal{F}_{\text{fuse}} \in \mathbb{R}^{N \times D}$) before fusion (Fig. 1a), inherently leads to the loss of valuable information due to compressing the total sequence length. In contrast, our proposed Sigma processes concatenated sequences, preserving all valuable information while requiring significantly less computation.

2.2 State Space Models

State Space Models (SSM) [17, 47], inspired by linear time-invariant (LTI) systems, are considered as efficient sequence-to-sequence models. Recently, the Structured State-Space Sequence model (S4) [17] has emerged as a pioneering work in deep state-space modeling, particularly for capturing long-range dependencies. Furthermore, with the selective mechanism introduced into S4, Mamba [16] surpasses Transformers and other advanced architectures. Due to the remarkable performance of SSM, researchers have extended it to the field of computer vision. Models such as ViS4mer [25], S4ND [39], TranS4mer [26] and the Selective S4 model [53] demonstrate the effective modeling of image sequences with S4. Recently, Vision Mamba [80] integrates SSM with bidirectional scanning, making each patch related to another. Meanwhile, VMamba [33] extends scanning in four directions to fully capture interrelations among image patches. Besides, state space models have been extended to medical image segmentation [38, 41, 56, 60], image restoration [19] and point cloud analysis [28], all showing competitive

results with lower complexity. However, recent works directly employ SSM as a plug-and-play module, without the in-depth design tailored to specific tasks. Additionally, there is a lack of exploration of SSM in multi-modal tasks. Thus, we propose an attention-based Mamba fusion mechanism and a channel-aware Mamba decoder, designed to effectively augment essential information from various modalities and seamlessly integrate them. By leveraging the specialized design of SSM for multi-modal tasks, our approach attains enhanced accuracy while maintaining low complexity.

3 Sigma: Siamese Mamba Network

In this section, we give a detailed illustration of our proposed **Siamese Mamba Network (Sigma)** for multi-modal semantic segmentation. To start, we provide basic information on State Space Models. Subsequently, we present an overview of our Sigma architecture, followed by in-depth discussions of the encoder, fusion module, and decoder.

3.1 Preliminaries

State Space Models. State Space Models (SSM) [17, 18, 47] represent a class of sequence-to-sequence modeling systems characterized by constant dynamics over time, a property also known as linear time-invariant (LTI). With linear complexity, SSM can effectively capture the inherent dynamics of systems through an implicit mapping to latent states, which can be defined as:

$$y(t) = Ch(t) + Dx(t), \dot{h}(t) = Ah(t) + Bx(t). \quad (1)$$

Here, $x(t) \in \mathbb{R}$, $h(t) \in \mathbb{R}^N$, and $y(t) \in \mathbb{R}$ denotes the input, hidden state, and the output, respectively. N is the state size, and $\dot{h}(t)$ refers to the time derivative of $h(t)$. Additionally, $A \in \mathbb{R}^{N \times N}$, $B \in \mathbb{R}^{N \times 1}$, $C \in \mathbb{R}^{1 \times N}$, and $D \in \mathbb{R}$ are the system matrices. To process discrete sequences like image and text, SSMs adopt zero-order hold (ZOH) discretization [17] to map the input sequence $\{x_1, x_2, \dots, x_K\}$ to the output sequence $\{y_1, y_2, \dots, y_K\}$. Specifically, suppose $\Delta \in \mathbb{R}^D$ is the pre-defined timescale parameter to map continuous parameters A, B into a discrete space, the discretization process can be formulated as:

$$\bar{A} = \exp(\Delta A), \bar{B} = (\Delta A)^{-1}(\exp(\Delta A) - I) \cdot \Delta B, \bar{C} = C, \quad (2)$$

$$y_k = \bar{C}h_k + \bar{D}x_k, h_k = \bar{A}h_{k-1} + \bar{B}x_k. \quad (3)$$

Here, all the matrices keep the same dimension as the operation iterates. Notably, \bar{D} , serving as a residual connection, is often discarded in the equation:

$$y_k = \bar{C}h_k. \quad (4)$$

Besides, following Mamba [16], the matrix \bar{B} can be approximated by the first-order Taylor series:

$$\bar{B} = (\exp(\Delta A) - I)A^{-1}B \approx (\Delta A)(\Delta A)^{-1}\Delta B = \Delta B \quad (5)$$

Selective Scan Mechanism. While SSM is effective for modeling discrete sequences, they encounter limitations due to their LTI property, which results in invariant parameters regardless of differences in the input. To address this limitation, the Selective State Space Model (S6, *a.k.a* Mamba) [16] is introduced, making State Space Models to be input-dependent. In Mamba, the matrices $B \in \mathbb{R}^{L \times N}$, $C \in \mathbb{R}^{L \times N}$, and $\Delta \in \mathbb{R}^{L \times D}$ are derived from the input data $x \in \mathbb{R}^{L \times D}$, enabling the model to be contextually aware of the input. With this selection mechanism, Mamba is capable of effectively modeling the complex interactions present in long sequences.

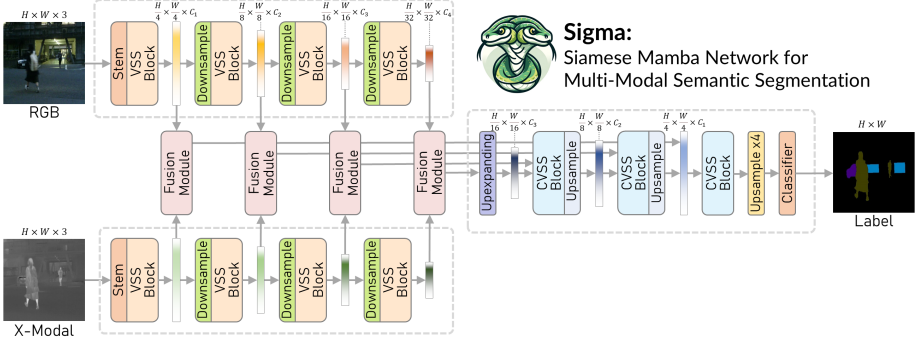


Fig. 2: Overall architecture of the proposed Sigma.

3.2 Overall Architecture

As illustrated in Fig. 2, our proposed method comprises a Siamese feature extractor (Sec. 3.3), a feature fusion module (Sec. 3.4), and an upsampling decoder (Sec. 3.5), forming an architecture entirely composed of State Space Models. During the encoding phase, four Visual State Space (VSS) Blocks with downsampling operations are sequentially cascaded to extract multi-level image features. The two encoder branches share weights to reduce computational complexity. Subsequently, features from each level, derived from two distinct branches, are processed through a fusion module. In the decoding phase, the fused features at each level are further enhanced by a Channel-Aware Visual State Space (CVSS) Block with an upsampling operation. Ultimately, the final feature is forwarded to a classifier to generate the outcome.

3.3 Siamese Mamba Encoder

Given a pair of multi-modal inputs, the X-modality input is pre-processed to the same dimension as the RGB image, which can be denoted as $I_{\text{RGB}}, I_{\text{X}} \in \mathbb{R}^{H \times W \times 3}$, where H and W represent the height and width of the input modalities. The encoder starts with a stem module similar to ViT [10] which partitions the input into patches, generating feature maps $\mathcal{F}_i^1 \in \mathbb{R}^{\frac{H}{4} \times \frac{W}{4} \times C_1}$, where $i \in \{\text{RGB}, \text{X}\}$ refers to the RGB or X modality. Then we apply a Visual State Space (VSS)

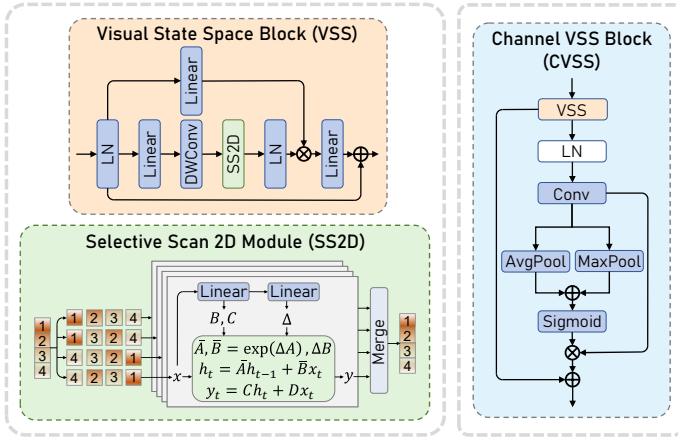


Fig. 3: The left part of the figure shows the Visual State Space (VSS) Block used in the Sigma encoder and its component, Selective Scan 2D (SS2D) module. The right part indicates the Channel-Aware VSS (CVSS) Block used in the Sigma decoder.

Block to process the features. This operation keeps the feature dimension unchanged. The features are continually processed by three sets of downsampling and VSS blocks, yielding multi-scale deep features $\{\mathcal{F}_i^2 \in \mathbb{R}^{\frac{H}{8} \times \frac{W}{8} \times C_2}, \mathcal{F}_i^3 \in \mathbb{R}^{\frac{H}{16} \times \frac{W}{16} \times C_3}, \mathcal{F}_i^4 \in \mathbb{R}^{\frac{H}{32} \times \frac{W}{32} \times C_4}\}$. The details of VSS Block are introduced as follows.

VSS Block. Following VMamba [33] and MambaIR [19], we implement the VSS Block with Selective Scan 2D (SS2D) modules. As shown in the left part of Fig. 3, the input feature is processed by a sequence of linear projection (Linear), Depth-wise Convolution (DWConv) as the original Mamba [16], and an SS2D module is used to model long-range spatial information from the feature followed by a residual connection.

SS2D Module. Within the SS2D module, the input feature of shape $\mathbb{R}^{H \times W \times C}$ is first flattened to four $\mathbb{R}^{(H \times W) \times C}$ sequences from four directions (top-left to bottom-right, bottom-right to top-left, top-right to bottom-left, and bottom-left to top-right) as proposed in [33]. Then four distinctive Selective Scan Modules [16] are used to extract multi-direction information, where each of them captures the long-range dependencies of the sequence with the operation in Eq. 3. Lastly, the four sequences are reversed to the same direction and summed.

3.4 Fusion Module

The detailed architecture of the feature fusion module is illustrated in Fig. 4, where the multi-modal features from the Siamese backbone are enhanced by a Cross Mamba Block (CroMB) followed by a Concat Mamba Block (ConMB).

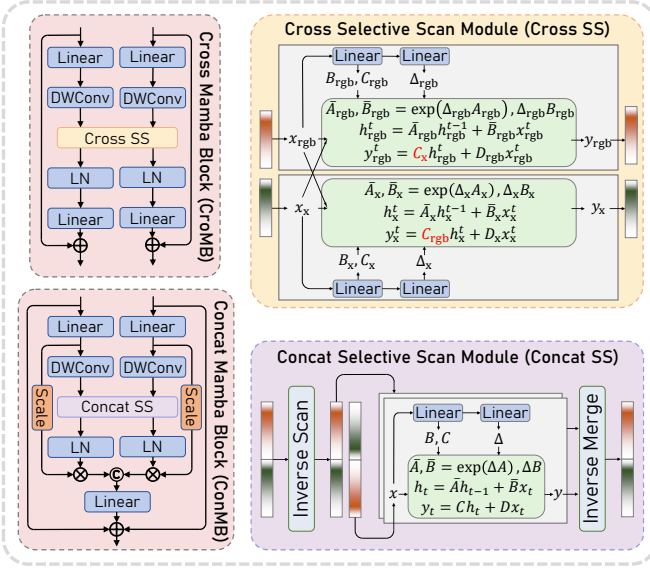


Fig. 4: The left part of the figure shows the Cross Mamba Block (CroMB) and Concat Mamba Block (ConMB). The right part shows the components of CroMB and ConMB respectively, namely Cross Selective Scan (Cross SS) Module and Concat Selective Scan (Concat SS) Module.

Specifically, CroMB employs a cross-multiplication mechanism to enhance the features with one another, and ConMB applies the Selective Scan mechanism to concatenated features to obtain the fusion result. Suppose the features from the k^{th} Siamese encoder block are represented as $\mathcal{F}_{\text{RGB}/X}^k \in \mathbb{R}^{H_k \times W_k \times C_k}$, then the entire fusion process can be represented as:

$$\hat{\mathcal{F}}_{\text{RGB}}, \hat{\mathcal{F}}_X^k = \text{CroMB}(\mathcal{F}_{\text{RGB}}^k, \mathcal{F}_X^k), \quad (6)$$

$$\mathcal{F}_{\text{Fuse}}^k = \text{ConMB}(\hat{\mathcal{F}}_{\text{RGB}}^k, \hat{\mathcal{F}}_X^k). \quad (7)$$

Here, $\hat{\mathcal{F}}_{\text{RGB}}, \hat{\mathcal{F}}_X^k$, and $\mathcal{F}_{\text{Fuse}}^k$ remains the original dimension as $\mathbb{R}^{H_k \times W_k \times C_k}$. Details of CroMB and ConMB are shown as follows.

CroMB. As demonstrated in the upper portion of Fig. 4, CroMB accepts two features as input and generates two outputs, preserving the original shape of the features. The two input features are first processed by linear layers and depth-wise convolutions respectively, then sent to the Cross Selective Scan (Cross SS) Module. According to the selection mechanism of Mamba mentioned in Sec. 3.1, the system matrices B, C and Δ are generated by the input to enable the context-aware ability of the model. Here, linear projection layers are utilized to generate the matrices. According to Eq. 4, matrix C is used to decode the information from the hidden state h_k to obtain the output y_k . Inspired by the cross-attention mechanism [3], which is extensively applied in multi-modal tasks, we

aim to facilitate information exchange among multiple Selective Scan Modules. To achieve this, we propose using the C matrix generated by the complementary modality in the Selective Scan operation, which enables the SSM to reconstruct output from the hidden state guided by another modality. In particular, the process can be represented as:

$$\bar{A}_{\text{rgb}} = \exp(\Delta_{\text{rgb}} A_{\text{rgb}}), \bar{A}_{\text{x}} = \exp(\Delta_{\text{x}} A_{\text{x}}), \quad (8)$$

$$\bar{B}_{\text{rgb}} = \Delta_{\text{rgb}} B_{\text{rgb}}, \bar{B}_{\text{x}} = \Delta_{\text{x}} B_{\text{x}}, \quad (9)$$

$$h_{\text{rgb}}^t = \bar{A}_{\text{rgb}} h_{\text{rgb}}^{t-1} + \bar{B}_{\text{rgb}} x_{\text{rgb}}^t, h_{\text{x}}^t = \bar{A}_{\text{x}} h_{\text{x}}^{t-1} + \bar{B}_{\text{x}} x_{\text{x}}^t, \quad (10)$$

$$y_{\text{rgb}}^t = C_{\text{x}} h_{\text{rgb}}^t + D_{\text{rgb}} x_{\text{rgb}}^t, y_{\text{x}}^t = C_{\text{rgb}} h_{\text{x}}^t + D_{\text{x}} x_{\text{x}}^t, \quad (11)$$

$$y_{\text{rgb}} = [y_{\text{rgb}}^1, y_{\text{rgb}}^2, \dots, y_{\text{rgb}}^l], y_{\text{x}} = [y_{\text{x}}^1, y_{\text{x}}^2, \dots, y_{\text{x}}^l]. \quad (12)$$

Here, $x_{\text{rgb}/\text{x}}^t$ represents the input at time step t , and $y_{\text{rgb}/\text{x}}$ denotes the selective scan output. C_{x} and C_{rgb} are the cross-modal matrices used for recovering the outputs at each time step from the hidden states.

ConMB. In CroMB, the features from two modalities interact with each other through the Cross Selective Scan operation and obtain the cross-modal-enhanced features. To further obtain a fused feature containing vital information from both modalities, we propose ConMB to integrate the outputs from CroMB. Due to the quadratic scaling property, previous Transformer-based methods often partition the input into small patches [10], which impedes the capture of information within each token. In contrast, leveraging the long-sequence modeling capability of Mamba, our ConMB directly processes the concatenated features as input, thereby preserving as much information from both modalities as possible.

Specifically, the outputs $\hat{\mathcal{F}}_{\text{RGB}}^k, \hat{\mathcal{F}}_{\text{X}}^k \in \mathbb{R}^{H_k \times W_k \times C_k}$ from CroMB are first processed by linear and convolution layers, then sent to the Concat Selective Scan (Concat SS) Module. Within the Concat SS Module, the two features are first flattened to $\mathbb{R}^{(H_k \times W_k) \times C_k}$ and then concatenated on the sequence length dimension. This provides a sequence $\mathcal{S}_{\text{Concat}}^k$ of shape $\mathbb{R}^{(2 \times H_k \times W_k) \times C_k}$. Besides, to comprehensively capture information from two modalities, we inversely scan the concatenated sequence $\mathcal{S}_{\text{Concat}}^k$ to get an additional sequence $\mathcal{S}_{\text{Inverse}}^k \in \mathbb{R}^{(2 \times H_k \times W_k) \times C_k}$. Afterwards, each sequence is processed by a 1D Selective Scan Module proposed in [16] to capture long-range dependencies from two modalities, obtaining $\hat{\mathcal{S}}_{\text{Concat}}^k$ and $\hat{\mathcal{S}}_{\text{Inverse}}^k$. Then the inversed sequence output is flipped back and added with the processed concatenated sequence. The summed sequence is separated to recover two outputs. This process can be represented as:

$$\tilde{\mathcal{F}}_{\text{RGB}}^k = \text{DWConv}(\text{Linear}(\hat{\mathcal{F}}_{\text{RGB}}^k)), \tilde{\mathcal{F}}_{\text{X}}^k = \text{DWConv}(\text{Linear}(\hat{\mathcal{F}}_{\text{X}}^k)), \quad (13)$$

$$\mathcal{S}_{\text{Concat}}^k = \text{Concat}(\tilde{\mathcal{F}}_{\text{RGB}}^k, \tilde{\mathcal{F}}_{\text{X}}^k, \text{dim} = 0), \quad (14)$$

$$\mathcal{S}_{\text{Inverse}}^k = \text{Inverse}(\mathcal{S}_{\text{Concat}}^k), \quad (15)$$

$$\hat{\mathcal{S}}_{\text{Concat}}^k, \hat{\mathcal{S}}_{\text{Inverse}}^k = \text{SSM}(\mathcal{S}_{\text{Concat}}^k), \text{SSM}(\mathcal{S}_{\text{Inverse}}^k), \quad (16)$$

$$\bar{\mathcal{F}}_{\text{RGB}}^k, \bar{\mathcal{F}}_{\text{X}}^k = \text{Separate}(\hat{\mathcal{S}}_{\text{Concat}}^k + \text{Inverse}(\hat{\mathcal{S}}_{\text{Inverse}}^k)). \quad (17)$$

After obtaining the scanned features $\overline{\mathcal{F}}_{\text{RGB}}^k, \overline{\mathcal{F}}_{\text{X}}^k$, they are multiplied with two scaling parameters derived from $\hat{\mathcal{F}}_{\text{RGB}}^k, \hat{\mathcal{F}}_{\text{X}}^k$ and concatenated on the channel dimension, forming a feature of shape $\mathbb{R}^{H_k \times W_k \times (2 \times C_k)}$. Finally, a linear projection layer is used to reduce the feature shape to $\mathbb{R}^{H_k \times W_k \times C_k}$.

3.5 Channel-Aware Mamba Decoder

State Space Models are adept at extracting global spatial context, yet they fall short in learning inter-channel information. To mitigate this issue, we propose a Channel-Aware Mamba decoder. As shown in the right portion of Fig. 3, CVSS Block first includes a VSS Block used in the encoder. After extracting the spatial long-range dependencies, a Channel-Attention operation consisting of Average Pooling and Max Pooling is introduced. In this manner, we form a spatial-channel-aware scheme that has been proven effective in [57].

4 Experiments

4.1 Experimental Settings

Datasets. To verify the effectiveness of Sigma, we conduct extensive experiments on two publicly available RGB-Thermal (RGB-T) semantic segmentation datasets, namely MFNet [21] and PST900 [45]. Besides, to better understand the generalization ability of Sigma to other multi-modal scene understanding tasks, we conduct experiments on two RGB-Depth (RGB-D) datasets, including NYU Depth V2 [46] and SUN RGB-D [48]. The details of these datasets are as follows.

- **MFNet dataset** contains 820 daytime and 749 nighttime RGB-T images with a resolution of 640×480 . The dataset includes eight common classes of objects in driving scenarios. We follow the training/testing split of [30].
- **PST900 dataset** provides 597 and 288 calibrated RGB-T images with a resolution of 1280×720 for training and validation. This dataset is collected from DARPA Subterranean Challenge and annotated with four classes.
- **NYU Depth V2 dataset** contains 1449 RGB Depth images annotated with 40 semantic classes with the shape of 640×480 . We divide them into 795/654 for training/testing following previous works [15, 24].
- **SUN RGB-D dataset** incorporates 10335 RGB-D images with 37 classes. We follow the common setting [24] to split 5285/5050 for training/testing, and reshape the images to 640×480 .

Evaluation. Following previous works [24, 73], we report the Intersection over Union (mIoU) averaged across the semantic classes for evaluation.

Table 1: Quantitative comparisons for semantic segmentation of RGB-T images on MFNet [21] and PST900 [45] datasets. The best and second best performance in each block is highlighted in **bold** and underline, respectively.

Method	Backbone	Params (M)	FLOPs (G)	Unlabeled	Car	Person	Bike	Curve	Car Stop	Guardrail	Cone	Bump	mIoU
MFNet ₁₇ [21]	–	–	–	96.9	65.9	58.9	42.9	29.9	9.9	0.0	25.2	27.7	39.7
RTFNet ₁₉ [49]	ResNet-152	245.7	185.2	<u>98.5</u>	87.4	70.3	62.7	45.3	29.8	0.0	29.1	55.7	53.2
PSTNet ₂₀ [45]	ResNet-18	105.8	123.4	97.0	76.8	52.6	55.3	29.6	25.1	15.1	39.4	45.0	48.4
FuseSeg ₅₀ [50]	DenseNet-161	141.5	193.4	97.6	87.9	71.7	64.6	44.8	22.7	6.4	46.9	47.9	54.5
U2Fusion ₂₉ [61]	VGG-16	–	–	97.7	82.8	64.8	61.0	32.3	20.9	–	45.2	50.2	50.8
AFNet ₂₁ [62]	ResNet-50	–	–	98.0	86.0	67.4	62.0	43.0	28.9	4.6	44.9	56.6	54.6
ABMDRNet ₂₁ [74]	ResNet-50	64.6	194.3	98.6	84.8	69.6	60.3	45.1	33.1	5.1	47.4	50.0	54.8
FEANet ₂₁ [7]	ResNet-152	337.1	255.2	98.3	87.8	71.1	61.1	46.5	22.1	6.6	55.3	48.9	55.3
GMNet ₂₁ [77]	ResNet-50	149.8	153.0	97.5	86.5	73.1	61.7	44.0	<u>42.3</u>	14.5	48.7	47.4	57.3
TarDAL ₂₂ [31]	–	297	–	97.6	80.7	67.1	60.1	34.9	10.5	–	38.7	45.5	48.6
CMX ₂₂ [30]	MiT-B4	139.9	134.3	98.3	90.1	75.2	64.5	50.2	35.3	8.5	54.2	<u>60.6</u>	59.7
EAEFNet ₂₃ [29]	ResNet-152	200.4	147.3	–	87.6	72.6	63.8	48.6	35.0	<u>14.2</u>	52.4	58.3	58.9
CACFNet ₂₃ [76]	ConvNeXt-B	198.6	101.4	–	89.2	69.5	63.3	46.6	32.4	7.9	54.9	58.3	57.8
PAIF ₂₃ [35]	–	260	–	–	88.1	72.4	60.8	–	–	–	<u>56.0</u>	57.2	56.5
CENet ₂₃ [3]	ResNet-50	–	–	–	85.8	70.0	61.4	46.8	29.3	8.7	47.8	56.9	56.1
SegMIF ₂₃ [32]	MiT-B3	–	–	–	98.1	87.8	71.4	63.2	47.5	31.1	–	48.9	50.3
CMNeXT ₂₃ [73]	MiT-B4	119.6	131.9	98.4	91.5	<u>75.3</u>	67.6	50.5	40.1	9.3	53.4	52.8	59.9
CAINet ₂₄ [37]	MobileNet-V2	12.16	123.62	–	88.5	66.3	68.7	55.4	31.5	9.0	48.9	60.7	58.6
Sigma (Ours)	VMamba-T	48.3	89.5	98.4	90.8	75.2	66.6	48.2	38.0	8.7	55.9	60.4	60.2
Sigma (Ours)	VMamba-S	69.8	138.9	<u>98.5</u>	91.5	75.8	67.8	49.6	41.8	9.6	54.8	60.4	<u>61.1</u>
Sigma (Ours)	VMamba-B	121.4	240.7	98.5	<u>91.1</u>	75.2	68.0	50.8	43.0	9.7	57.6	57.9	61.3

(a) Quantitative comparison on MFNet day-night evaluation set [21] (9 classes)

Method	Backbone	Background	Extinguisher	Backpack	Hand-Drill	Survivor	mIoU
MFNet ₁₇ [21]	–	98.6	60.4	64.3	41.1	20.7	57.0
RTFNet ₁₉ [49]	ResNet-152	98.9	52.0	75.3	25.4	36.4	57.6
PSTNet ₂₀ [45]	ResNet-18	98.9	70.1	69.2	53.6	50.0	68.4
ABMDRNet ₂₁ [74]	ResNet-50	99.0	66.2	67.9	61.5	62.0	71.3
GMNet ₂₁ [77]	ResNet-50	99.4	73.8	83.8	85.2	78.4	84.1
CCFFNet ₂₂ [58]	ResNet-101	99.4	82.8	75.8	79.9	72.7	82.1
EGFNet ₂₃ [8]	ResNet-101	99.6	80.0	90.6	76.1	80.9	85.4
CACFNet ₂₃ [76]	ConvNeXt-B	99.6	<u>82.1</u>	89.5	80.9	80.8	86.6
CAINet ₂₄ [37]	MobileNet-V2	<u>99.5</u>	80.3	88.0	77.2	78.7	84.7
Sigma (Ours)	VMamba-T	99.6	81.9	<u>89.8</u>	<u>88.7</u>	82.7	88.6
Sigma (Ours)	VMamba-S	99.6	79.4	88.7	90.2	<u>81.2</u>	<u>87.8</u>

(b) Quantitative comparison on PST900 evaluation set [45] (5 classes)

Training Settings. We follow [30] to use the AdamW optimizer [36] with an initial learning rate $6e^{-5}$ and weight decay 0.01. The model is trained with a batch size of 8 for 500 epochs. We utilize the ImageNet-1K [42] pre-trained model provided by VMamba [33] for the Siamese image encoder, leading to three different sizes of models (Sigma-Tiny, Sigma-Small, and Sigma-Base). For the tiny and small model, we use four NVIDIA RTX 3090 GPUs for training. For the base model, we use four NVIDIA RTX A6000 GPUs for training. All the models are evaluated with a single NVIDIA RTX 3090 GPU. More details about the experimental settings are described in the appendix.

4.2 Quantitative and Qualitative Results

RGB-T Semantic Segmentation. Tab. 1(a) shows the per-class semantic segmentation results, alongside comparisons of model size and computational complexity, on the MFNet dataset. It is observed that our tiny model surpasses other compared methods with fewer model parameters and FLOPs, and our base model achieves a 1.1% performance improvement compared to the tiny variant. Besides, as shown in Tab. 1(b), our method outperforms other methods by more

Table 2: Comparison of RGB-D Semantic Segmentation on NYU Depth V2 [46] and SUN RGB-D [48]. † indicates the parameters for multi-task learning reported from [68].

Method	Backbone	Params (M)	NYU Depth V2		SUN RGB-D	
			Input Size	mIoU	Input Size	mIoU
ACNet ₁₉ [24]	ResNet-50	116.6	480 × 640	48.3	530 × 730	48.1
SA-Gate ₂₀ [6]	ResNet-101	110.9	480 × 640	52.4	530 × 730	49.4
CEN ₂₀ [55]	ResNet-101	118.2	480 × 640	51.7	530 × 730	50.2
CEN ₂₀ [55]	ResNet-152	133.9	480 × 640	52.5	530 × 730	51.1
SGNet ₂₁ [5]	ResNet-101	64.7	480 × 640	51.1	530 × 730	48.6
ShapeConv ₂₁ [2]	ResNext-101	86.8	480 × 640	51.3	530 × 730	48.6
ESANet ₂₁ [44]	ResNet-34	31.2	480 × 640	50.3	480 × 640	48.2
FRNet ₂₂ [79]	ResNet-34	85.5	480 × 640	53.6	530 × 730	51.8
PGDENet ₂₂ [78]	ResNet-34	100.7	480 × 640	53.7	530 × 730	51.0
EMSANet ₂₂ [43]	ResNet-34	46.9	480 × 640	51.0	530 × 730	48.4
TokenFusion ₂₂ [54]	MiT-B2	26.0	480 × 640	53.3	530 × 730	50.3
TokenFusion ₂₂ [54]	MiT-B3	45.9	480 × 640	54.2	530 × 730	51.0
MultiMAE ₂₂ [1]	ViT-B	95.2	640 × 640	56.0	640 × 640	51.1
Omnivore ₂₂ [15]	Swin-B	95.7	480 × 640	54.0	–	–
PDCNet ₂₃ [64]	ResNet-101	–	480 × 480	53.5	480 × 480	49.6
InvPT ₂₃ [67]	ViT-L	423 [†]	480 × 640	53.6	–	–
TaskPrompter ₂₃ [68]	TaskPrompter-L	401 [†]	480 × 640	55.3	–	–
SMMCL ₂₄ [9]	SegNeXt-B	–	480 × 640	55.8	–	–
CMNeXt ₂₃ [73]	MiT-B4	119.6	480 × 640	<u>56.9</u>	530 × 730	<u>51.9</u>
CAINet ₂₄ [37]	MobileNet-V2	12.2	480 × 640	52.6	–	–
Sigma (Ours)	VMamba-T	48.3	480 × 640	53.9	480 × 640	50.0
Sigma (Ours)	VMamba-S	69.8	480 × 640	57.0	480 × 640	52.4

than 2% on PST900 [45] dataset, demonstrating the superiority of our proposed method.

The qualitative analysis illustrated in Fig. 5 reveals that our Sigma model outperforms baseline models by generating more precise segmentations and accurate classifications, notably in identifying intricate features like tactile paving and bollards. The enhanced outcomes stem from Sigma’s ability to extract valuable information from both RGB and thermal modalities. Specifically, RGB enhances color distinction, whereas thermal imaging excels in texture differentiation. Integrating these modalities results in improved segmentation accuracy.

RGB-D Semantic Segmentation. In Table 2, we compare Sigma against various RGB-D methods to validate Sigma’s generalization capability across different multi-modal segmentation tasks. Remarkably, our Sigma-S model surpasses the performance of CMNeXt [73] while employing only 69.8M parameters, which is 49.8M less than CMNeXt. This demonstrates the superior balance our proposed method achieves between accuracy and efficiency.

Fig. 6 demonstrates Sigma’s capability to generate more coherent segmentation by utilizing depth information effectively. For instance, in the case of the round chair adjacent to the sofa, shadows cause baseline models to fragment the chair into multiple segments. Sigma successfully recognizes it as a singular entity, highlighting its superior proficiency in leveraging depth data for segmentation.

4.3 Ablation Studies

As detailed in Table 3, we carried out ablation studies with Sigma-Tiny on the MFNet [21] dataset by omitting the components we introduced. Compared

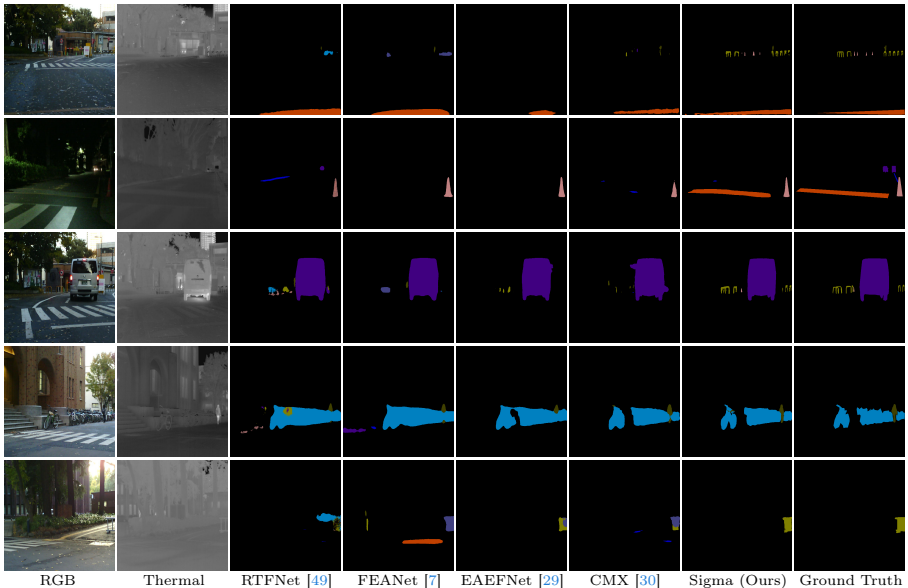


Fig. 5: Qualitative comparison on MFNet [21] dataset.

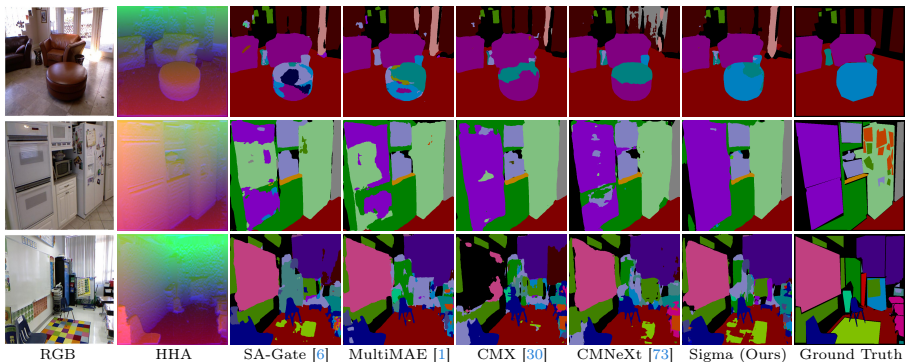


Fig. 6: Qualitative comparison on NYU Depth V2 [46] dataset. We use HHA images for better visualization of depth modality.

to the complete Sigma model, eliminating the Cross Mamba Block (CroMB) and Concat Mamba Block (ConMB) individually results in decreases of 0.6% and 0.8% in performance, respectively. The removal of both blocks leads to a performance decline of 2.1%, highlighting the effectiveness of our proposed fusion module. Additionally, we evaluate our proposed decoder against a simple Multi-Layer Perceptron (MLP) decoder and a Swin-Transform decoder, discovering that our decoder surpasses them by 1.1% and 0.9%, respectively. In our final analysis, to assess the efficacy of Mamba compared to other Transformer-based architectures, such as the Swin Transformer, we substitute our encoder with a pre-trained Swin Transformer [34] Tiny backbone and apply Swin Transformer blocks in the decoder. This outcome suggests that our design with SSM can be more effective than a simple integration of Transformers.

Table 3: Ablation studies on the MFNet [21] dataset. We report the mIoU metric and the relative decrease (∇) in blue. The Encoder column applies either VMamba Tiny or Swin-Transformer Tiny for feature extraction, and the decoder column indicates using the Channel-Aware Mamba Decoder, MLP decoder, or Swin Transformer decoder. When both CroMB and ConMB show \times marks, we use a simple feature summation operation to obtain the fused feature.

#	Encoder	CroMB	ConMB	Decoder	mIoU (∇)
1	VMamba-T	✓	✓	CMD	60.5 (0.0)
2	VMamba-T	✗	✓	CMD	59.9 (-0.6)
3	VMamba-T	✓	✗	CMD	59.7 (-0.8)
4	VMamba-T	✗	✗	CMD	58.4 (-2.1)
5	VMamba-T	✓	✓	MLP	59.4 (-1.1)
6	VMamba-T	✗	✗	MLP	57.5 (-3.0)
7	VMamba-T	✓	✓	Swin	59.6 (-0.9)
8	Swin-T	✗	✗	Swin	56.3 (-4.2)

5 Conclusion

In this work, we propose Sigma, a novel Siamese Mamba Network for multi-modal semantic segmentation, which explores the application of State Space Models in multi-modal scene understanding for the first time. A Siamese backbone consisting of a 2D selective scan mechanism is first applied to extract robust global long-range dependencies with linear complexity. Then we introduce a fusion module incorporating a cross-selective scan and a concat-selective scan operation. Finally, we design a channel-aware Mamba decoder to extract essential information from the fused features for predictions. Extensive experiments on RGB-Thermal and RGB-Depth semantic segmentation benchmarks show the superiority of Sigma in both accuracy and efficiency.

Limitations and Future Works. While Sigma has achieved outstanding results in various RGB-X semantic segmentation tasks, two limitations remain. 1) *Underutilization of Mamba for Longer Sequences:* Mamba’s capability to handle extremely long sequences is a significant advantage, particularly beneficial in fusion tasks involving more than two modalities. However, our current exploration primarily focuses on the application of Mamba for two modalities, potentially not fully leveraging its capacity for modeling longer sequences. Future work will aim to investigate Mamba’s performance on datasets with a greater variety of modalities, such as the DELIVER benchmark [73]. This exploration is pivotal for advancing research on enabling autonomous agents to navigate environments using multiple sensors, including RGB, depth, thermal, and LiDAR. 2) *Memory Consumption in the Mamba Encoder:* The Mamba encoder scans image features from four directions, allowing each pixel to assimilate information from its surrounding pixels. This approach, however, quadruples memory usage, posing a challenge for deployment on lightweight edge devices. Future endeavors will seek to incorporate positional information through alternative methods, such as positional encoders, and employ a 1D SSM to diminish computational and memory demands.

Acknowledgement

This work has been funded in part by the Army Research Laboratory (ARL) under grant W911NF-23-2-0007 and W911NF-19-2-0146, and the Air Force Office of Scientific Research (AFOSR) under grants FA9550-18-1-0097 and FA9550-18-1-0251.

References

1. Bachmann, R., Mizrahi, D., Atanov, A., Zamir, A.: Multima: Multi-modal multi-task masked autoencoders. In: European Conference on Computer Vision. pp. 348–367. Springer (2022) [2](#), [4](#), [12](#), [13](#), [20](#)
2. Cao, J., Leng, H., Lischinski, D., Cohen-Or, D., Tu, C., Li, Y.: Shapeconv: Shape-aware convolutional layer for indoor rgb-d semantic segmentation. In: Proceedings of the IEEE/CVF international conference on computer vision. pp. 7088–7097 (2021) [12](#)
3. Chen, C.F.R., Fan, Q., Panda, R.: Crossvit: Cross-attention multi-scale vision transformer for image classification. In: Proceedings of the IEEE/CVF international conference on computer vision. pp. 357–366 (2021) [8](#)
4. Chen, L., Boardley, B., Hu, P., Wang, Y., Pu, Y., Jin, X., Yao, Y., Gong, R., Li, B., Huang, G., et al.: 2023 low-power computer vision challenge (lpcvc) summary. arXiv preprint arXiv:2403.07153 (2024) [1](#)
5. Chen, L.Z., Lin, Z., Wang, Z., Yang, Y.L., Cheng, M.M.: Spatial information guided convolution for real-time rgbd semantic segmentation. *IEEE Transactions on Image Processing* **30**, 2313–2324 (2021) [12](#)
6. Chen, X., Lin, K.Y., Wang, J., Wu, W., Qian, C., Li, H., Zeng, G.: Bi-directional cross-modality feature propagation with separation-and-aggregation gate for rgb-d semantic segmentation. In: European Conference on Computer Vision. pp. 561–577. Springer (2020) [12](#), [13](#), [20](#)
7. Deng, F., Feng, H., Liang, M., Wang, H., Yang, Y., Gao, Y., Chen, J., Hu, J., Guo, X., Lam, T.L.: Feanet: Feature-enhanced attention network for rgb-thermal real-time semantic segmentation. In: 2021 IEEE/RSJ International Conference on Intelligent Robots and Systems (IROS). pp. 4467–4473. IEEE (2021) [11](#), [13](#)
8. Dong, S., Zhou, W., Xu, C., Yan, W.: Egfnet: Edge-aware guidance fusion network for rgb-thermal urban scene parsing. *IEEE Transactions on Intelligent Transportation Systems* (2023) [11](#)
9. Dong, X., Yokoya, N.: Understanding dark scenes by contrasting multi-modal observations. In: Proceedings of the IEEE/CVF Winter Conference on Applications of Computer Vision. pp. 840–850 (2024) [12](#)
10. Dosovitskiy, A., Beyer, L., Kolesnikov, A., Weissenborn, D., Zhai, X., Unterthiner, T., Dehghani, M., Minderer, M., Heigold, G., Gelly, S., et al.: An image is worth 16x16 words: Transformers for image recognition at scale. arXiv preprint arXiv:2010.11929 (2020) [6](#), [9](#)
11. Fayyad, J., Jaradat, M.A., Gruyer, D., Najjaran, H.: Deep learning sensor fusion for autonomous vehicle perception and localization: A review. *Sensors* **20**(15), 4220 (2020) [3](#)
12. Feng, D., Haase-Schütz, C., Rosenbaum, L., Hertlein, H., Glaeser, C., Timm, F., Wiesbeck, W., Dietmayer, K.: Deep multi-modal object detection and semantic segmentation for autonomous driving: Datasets, methods, and challenges. *IEEE Transactions on Intelligent Transportation Systems* **22**(3), 1341–1360 (2020) [2](#), [3](#)

13. Feng, Z., Guo, Y., Sun, Y.: Cekd: Cross-modal edge-privileged knowledge distillation for semantic scene understanding using only thermal images. *IEEE Robotics and Automation Letters* **8**(4), 2205–2212 (2023) [2](#), [3](#), [11](#)
14. Gade, R., Moeslund, T.B.: Thermal cameras and applications: a survey. *Machine vision and applications* **25**, 245–262 (2014) [3](#)
15. Girdhar, R., Singh, M., Ravi, N., van der Maaten, L., Joulin, A., Misra, I.: Omnivore: A single model for many visual modalities. In: *Proceedings of the IEEE/CVF Conference on Computer Vision and Pattern Recognition*. pp. 16102–16112 (2022) [10](#), [12](#)
16. Gu, A., Dao, T.: Mamba: Linear-time sequence modeling with selective state spaces. *arXiv preprint arXiv:2312.00752* (2023) [2](#), [4](#), [5](#), [6](#), [7](#), [9](#)
17. Gu, A., Goel, K., Ré, C.: Efficiently modeling long sequences with structured state spaces. *arXiv preprint arXiv:2111.00396* (2021) [4](#), [5](#)
18. Gu, A., Johnson, I., Goel, K., Saab, K., Dao, T., Rudra, A., Ré, C.: Combining recurrent, convolutional, and continuous-time models with linear state space layers. *Advances in neural information processing systems* **34**, 572–585 (2021) [5](#)
19. Guo, H., Li, J., Dai, T., Ouyang, Z., Ren, X., Xia, S.T.: Mambair: A simple baseline for image restoration with state-space model (2024) [4](#), [7](#)
20. Guo, Y., Liu, Y., Georgiou, T., Lew, M.S.: A review of semantic segmentation using deep neural networks. *International journal of multimedia information retrieval* **7**, 87–93 (2018) [1](#)
21. Ha, Q., Watanabe, K., Karasawa, T., Ushiku, Y., Harada, T.: Mfnet: Towards real-time semantic segmentation for autonomous vehicles with multi-spectral scenes. pp. 5108–5115 (2017) [3](#), [10](#), [11](#), [12](#), [13](#), [14](#), [21](#), [22](#)
22. Hazirbas, C., Ma, L., Domokos, C., Cremers, D.: Fusetnet: Incorporating depth into semantic segmentation via fusion-based cnn architecture. In: *Asian conference on computer vision*. pp. 213–228. Springer (2016) [21](#)
23. He, K., Chen, X., Xie, S., Li, Y., Dollár, P., Girshick, R.: Masked autoencoders are scalable vision learners. In: *Proceedings of the IEEE/CVF conference on computer vision and pattern recognition*. pp. 16000–16009 (2022) [4](#)
24. Hu, X., Yang, K., Fei, L., Wang, K.: Acnet: Attention based network to exploit complementary features for rgb-d semantic segmentation. In: *2019 IEEE International Conference on Image Processing (ICIP)*. pp. 1440–1444. IEEE (2019) [10](#), [12](#)
25. Islam, M.M., Bertasius, G.: Long movie clip classification with state-space video models. In: *ECCV*. pp. 87–104. Springer (2022) [4](#)
26. Islam, M.M., Hasan, M., Athrey, K.S., Braskich, T., Bertasius, G.: Efficient movie scene detection using state-space transformers. In: *CVPR*. pp. 18749–18758 (2023) [4](#)
27. Kingma, D.P., Ba, J.: Adam: A method for stochastic optimization. In: *ICLR* (2015) [20](#)
28. Liang, D., Zhou, X., Wang, X., Zhu, X., Xu, W., Zou, Z., Ye, X., Bai, X.: Pointmamba: A simple state space model for point cloud analysis (2024) [2](#), [4](#)
29. Liang, M., Hu, J., Bao, C., Feng, H., Deng, F., Lam, T.L.: Explicit attention-enhanced fusion for rgb-thermal perception tasks. *IEEE Robotics and Automation Letters* (2023) [2](#), [4](#), [11](#), [13](#)
30. Liu, H., Zhang, J., Yang, K., Hu, X., Stiefelhagen, R.: Cmx: Cross-modal fusion for rgb-x semantic segmentation with transformers. *arXiv preprint arXiv:2203.04838* (2022) [2](#), [4](#), [10](#), [11](#), [13](#), [20](#), [21](#)

31. Liu, J., Fan, X., Huang, Z., Wu, G., Liu, R., Zhong, W., Luo, Z.: Target-aware dual adversarial learning and a multi-scenario multi-modality benchmark to fuse infrared and visible for object detection. In: Proceedings of the IEEE/CVF Conference on Computer Vision and Pattern Recognition. pp. 5802–5811 (2022) [11](#)
32. Liu, J., Liu, Z., Wu, G., Ma, L., Liu, R., Zhong, W., Luo, Z., Fan, X.: Multi-interactive feature learning and a full-time multi-modality benchmark for image fusion and segmentation. In: Proceedings of the IEEE/CVF international conference on computer vision. pp. 8115–8124 (2023) [4](#), [11](#)
33. Liu, Y., Tian, Y., Zhao, Y., Yu, H., Xie, L., Wang, Y., Ye, Q., Liu, Y.: Vmamba: Visual state space model. arXiv preprint arXiv:2401.10166 (2024) [2](#), [4](#), [7](#), [11](#), [20](#)
34. Liu, Z., Lin, Y., Cao, Y., Hu, H., Wei, Y., Zhang, Z., Lin, S., Guo, B.: Swin transformer: Hierarchical vision transformer using shifted windows. In: CVPR. pp. 10012–10022 (2021) [13](#)
35. Liu, Z., Liu, J., Zhang, B., Ma, L., Fan, X., Liu, R.: Paif: Perception-aware infrared-visible image fusion for attack-tolerant semantic segmentation. In: Proceedings of the 31st ACM International Conference on Multimedia. pp. 3706–3714 (2023) [11](#)
36. Loshchilov, I., Hutter, F.: Decoupled weight decay regularization. arXiv preprint arXiv:1711.05101 (2017) [11](#)
37. Lv, Y., Liu, Z., Li, G.: Context-aware interaction network for rgb-t semantic segmentation. IEEE Transactions on Multimedia (2024) [2](#), [11](#), [12](#)
38. Ma, J., Li, F., Wang, B.: U-mamba: Enhancing long-range dependency for biomedical image segmentation. arXiv preprint arXiv:2401.04722 (2024) [2](#), [4](#)
39. Nguyen, E., Goel, K., Gu, A., Downs, G., Shah, P., Dao, T., Baccus, S., Ré, C.: S4nd: Modeling images and videos as multidimensional signals with state spaces. Advances in neural information processing systems **35**, 2846–2861 (2022) [4](#)
40. Pohlen, T., Hermans, A., Mathias, M., Leibe, B.: Full-resolution residual networks for semantic segmentation in street scenes. In: CVPR (2017) [21](#)
41. Ruan, J., Xiang, S.: Vm-unet: Vision mamba unet for medical image segmentation. arXiv preprint arXiv:2402.02491 (2024) [2](#), [4](#)
42. Russakovsky, O., Deng, J., Su, H., Krause, J., Satheesh, S., Ma, S., Huang, Z., Karpathy, A., Khosla, A., Bernstein, M., et al.: Imagenet large scale visual recognition challenge. International journal of computer vision **115**, 211–252 (2015) [11](#), [20](#)
43. Seichter, D., Fishedick, S.B., Köhler, M., Groß, H.M.: Efficient multi-task rgb-d scene analysis for indoor environments. In: 2022 International Joint Conference on Neural Networks (IJCNN). pp. 1–10. IEEE (2022) [12](#)
44. Seichter, D., Köhler, M., Lewandowski, B., Wengefeld, T., Gross, H.M.: Efficient rgb-d semantic segmentation for indoor scene analysis. In: 2021 IEEE international conference on robotics and automation (ICRA). pp. 13525–13531. IEEE (2021) [12](#)
45. Shivakumar, S.S., Rodrigues, N., Zhou, A., Miller, I.D., Kumar, V., Taylor, C.J.: Pst900: Rgb-thermal calibration, dataset and segmentation network. In: 2020 IEEE international conference on robotics and automation (ICRA). pp. 9441–9447. IEEE (2020) [3](#), [10](#), [11](#), [12](#)
46. Silberman, N., Hoiem, D., Kohli, P., Fergus, R.: Indoor segmentation and support inference from rgb-d images. In: Computer Vision—ECCV 2012: 12th European Conference on Computer Vision, Florence, Italy, October 7–13, 2012, Proceedings, Part V 12. pp. 746–760. Springer (2012) [3](#), [10](#), [12](#), [13](#), [20](#)
47. Smith, J.T., Warrington, A., Linderman, S.W.: Simplified state space layers for sequence modeling. arXiv preprint arXiv:2208.04933 (2022) [4](#), [5](#)

48. Song, S., Lichtenberg, S.P., Xiao, J.: Sun rgb-d: A rgb-d scene understanding benchmark suite. In: Proceedings of the IEEE conference on computer vision and pattern recognition. pp. 567–576 (2015) [3](#), [10](#), [12](#), [20](#)
49. Sun, Y., Zuo, W., Liu, M.: Rtfnet: Rgb-thermal fusion network for semantic segmentation of urban scenes **4**(3), 2576–2583 (2019) [3](#), [11](#), [13](#), [21](#)
50. Sun, Y., Zuo, W., Yun, P., Wang, H., Liu, M.: Fuseseg: Semantic segmentation of urban scenes based on rgb and thermal data fusion. IEEE Trans. on Automation Science and Engineering (TASE) (2020) [3](#), [4](#), [11](#), [21](#)
51. Szegedy, C., Vanhoucke, V., Ioffe, S., Shlens, J., Wojna, Z.: Rethinking the inception architecture for computer vision. In: CVPR. pp. 2818–2826 (2016) [4](#)
52. Vaswani, A., Shazeer, N., Parmar, N., Uszkoreit, J., Jones, L., Gomez, A.N., Kaiser, Ł., Polosukhin, I.: Attention is all you need. NeurIPS **30** (2017) [2](#)
53. Wang, J., Zhu, W., Wang, P., Yu, X., Liu, L., Omar, M., Hamid, R.: Selective structured state-spaces for long-form video understanding. In: CVPR. pp. 6387–6397 (2023) [4](#)
54. Wang, Y., Chen, X., Cao, L., Huang, W., Sun, F., Wang, Y.: Multimodal token fusion for vision transformers. In: Proceedings of the IEEE/CVF Conference on Computer Vision and Pattern Recognition. pp. 12186–12195 (2022) [12](#), [20](#)
55. Wang, Y., Huang, W., Sun, F., Xu, T., Rong, Y., Huang, J.: Deep multimodal fusion by channel exchanging. Advances in neural information processing systems **33**, 4835–4845 (2020) [12](#)
56. Wang, Z., Ma, C.: Weak-mamba-unet: Visual mamba makes cnn and vit work better for scribble-based medical image segmentation (2024) [2](#), [4](#)
57. Woo, S., Park, J., Lee, J.Y., Kweon, I.S.: Cbam: Convolutional block attention module. In: Proceedings of the European conference on computer vision (ECCV). pp. 3–19 (2018) [10](#)
58. Wu, W., Chu, T., Liu, Q.: Complementarity-aware cross-modal feature fusion network for rgb-t semantic segmentation. Pattern Recognition **131**, 108881 (2022) [11](#)
59. Xie, E., Wang, W., Yu, Z., Anandkumar, A., Alvarez, J.M., Luo, P.: Segformer: Simple and efficient design for semantic segmentation with transformers. Advances in Neural Information Processing Systems **34**, 12077–12090 (2021) [4](#), [21](#)
60. Xing, Z., Ye, T., Yang, Y., Liu, G., Zhu, L.: Segmamba: Long-range sequential modeling mamba for 3d medical image segmentation. arXiv preprint arXiv:2401.13560 (2024) [2](#), [4](#)
61. Xu, H., Ma, J., Jiang, J., Guo, X., Ling, H.: U2fusion: A unified unsupervised image fusion network. IEEE Transactions on Pattern Analysis and Machine Intelligence **44**(1), 502–518 (2020) [3](#), [11](#)
62. Xu, J., Lu, K., Wang, H.: Attention fusion network for multi-spectral semantic segmentation. Pattern Recognition Letters **146**, 179–184 (2021) [3](#), [11](#)
63. Yan, T., Wan, Z., Zhang, P., Cheng, G., Lu, H.: Transy-net: Learning fully transformer networks for change detection of remote sensing images. IEEE Transactions on Geoscience and Remote Sensing (2023) [2](#)
64. Yang, J., Bai, L., Sun, Y., Tian, C., Mao, M., Wang, G.: Pixel difference convolutional network for rgb-d semantic segmentation. IEEE Transactions on Circuits and Systems for Video Technology pp. 1–1 (2023). <https://doi.org/10.1109/TCSVT.2023.3296162> [12](#)
65. Yang, Y., Xing, Z., Zhu, L.: Vivim: a video vision mamba for medical video object segmentation (2024) [2](#)

66. Yang, Y.Q., Guo, Y.X., Xiong, J.Y., Liu, Y., Pan, H., Wang, P.S., Tong, X., Guo, B.: Swin3d: A pretrained transformer backbone for 3d indoor scene understanding (2023) [2](#)
67. Ye, H., Xu, D.: Inverted pyramid multi-task transformer for dense scene understanding. In: ECCV (2022) [12](#)
68. Ye, H., Xu, D.: Taskprompter: Spatial-channel multi-task prompting for dense scene understanding. In: ICLR (2023) [12](#)
69. Yu, C., Wang, J., Peng, C., Gao, C., Yu, G., Sang, N.: Bisenet: Bilateral segmentation network for real-time semantic segmentation. In: Proceedings of the European conference on computer vision (ECCV). pp. 325–341 (2018) [21](#)
70. Yu, C., Wang, J., Peng, C., Gao, C., Yu, G., Sang, N.: Learning a discriminative feature network for semantic segmentation. In: CVPR (2018) [21](#)
71. Zhang, C., Stepputtis, S., Campbell, J., Sycara, K., Xie, Y.: Robust hierarchical scene graph generation. In: NeurIPS 2023 Workshop: New Frontiers in Graph Learning (2023) [1](#)
72. Zhang, C., Stepputtis, S., Campbell, J., Sycara, K., Xie, Y.: Hiker-sgg: Hierarchical knowledge enhanced robust scene graph generation. In: IEEE/CVF Conference on Computer Vision and Pattern Recognition (2024) [1](#)
73. Zhang, J., Liu, R., Shi, H., Yang, K., Reiß, S., Peng, K., Fu, H., Wang, K., Stiefelhagen, R.: Delivering arbitrary-modal semantic segmentation. In: Proceedings of the IEEE/CVF Conference on Computer Vision and Pattern Recognition. pp. 1136–1147 (2023) [2](#), [4](#), [10](#), [11](#), [12](#), [13](#), [14](#), [20](#)
74. Zhang, Q., Zhao, S., Luo, Y., Zhang, D., Huang, N., Han, J.: Abmdrnet: Adaptive-weighted bi-directional modality difference reduction network for rgb-t semantic segmentation. In: Proceedings of the IEEE/CVF Conference on Computer Vision and Pattern Recognition. pp. 2633–2642 (2021) [11](#)
75. Zhang, Y., Sidibé, D., Morel, O., Mériaudeau, F.: Deep multimodal fusion for semantic image segmentation: A survey. *Image and Vision Computing* **105**, 104042 (2021) [3](#)
76. Zhou, W., Dong, S., Fang, M., Yu, L.: Cacfnets: Cross-modal attention cascaded fusion network for rgb-t urban scene parsing. *IEEE Transactions on Intelligent Vehicles* (2023) [3](#), [11](#)
77. Zhou, W., Liu, J., Lei, J., Yu, L., Hwang, J.N.: Gmnet: graded-feature multilabel-learning network for rgb-thermal urban scene semantic segmentation. *IEEE Transactions on Image Processing* **30**, 7790–7802 (2021) [3](#), [4](#), [11](#), [21](#)
78. Zhou, W., Yang, E., Lei, J., Wan, J., Yu, L.: Pgdenet: Progressive guided fusion and depth enhancement network for rgb-d indoor scene parsing. *IEEE Transactions on Multimedia* (2022) [12](#)
79. Zhou, W., Yang, E., Lei, J., Yu, L.: Frnet: Feature reconstruction network for rgb-d indoor scene parsing. *IEEE Journal of Selected Topics in Signal Processing* **16**(4), 677–687 (2022) [12](#)
80. Zhu, L., Liao, B., Zhang, Q., Wang, X., Liu, W., Wang, X.: Vision mamba: Efficient visual representation learning with bidirectional state space model. *arXiv preprint arXiv:2401.09417* (2024) [4](#)

Sigma: Siamese Mamba Network for Multi-Modal Semantic Segmentation

Supplementary Material

A Experimental Details

During training, we perform data augmentation, including random flipping and scaling with random scales $[0.5, 1.75]$, to all datasets. We adopt VMamba [33] pre-trained on ImageNet [42] as the backbone, which includes three versions, namely VMamba-Tiny, VMamba-Small, and VMamba-Base. The detailed settings of the three models are listed in Tab. A1. We select AdamW optimizer [27] with weight decay 0.01. The original learning rate is set to $6e^{-5}$ and we employ a poly learning rate schedule with 10 warm-up epochs. We use cross-entropy as the loss function. When reporting testing results on NYU Depth V2 [46] and SUN RGB-D [48] datasets, we use multiple scales $\{0.75, 1, 1.25\}$ according to most previous RGB-Depth semantic segmentation methods [30, 73]. We use mean Intersection over Union (mIoU) averaged across semantic classes as the evaluation metric to measure the segmentation performance. For each of the datasets, more implementation details are described as follows.

MFNet dataset. The tiny and small backbones are trained on four 3090Ti GPUs and the base backbone is trained on four A6000 GPUs. We use the original image size of 640×480 for training and inference. The batch size is set to 8 for training. A single 3090Ti GPU is used for inferencing all the models.

PST900 dataset. The tiny and small backbones are trained on two A6000 GPUs. We use the original image size of 1280×720 for training and inference. The batch size is set to 4 for training. A single A6000 GPU is used for inferencing all the models.

NYU Depth V2 dataset. Unlike other methods [6, 30] to use HHA format of depth images for training, we directly use raw depth images and we found no apparent performance difference between the formats. We take the whole image with the size 640×480 for training and inference. 4 3090Ti GPUs are used to train the tiny and small backbones with batch size 8, and 4 A6000 GPUs are used to train the base model.

SUN-RGBD dataset. Unlike previous methods which use larger resolution input (730×530 [54, 73] or 640×640 [1]), we adopt the input resolution of 640×480 and keep the same training settings as NYU Depth V2 dataset. We also use raw depth images instead of HHA format for training.

Table A1: Details about three versions of backbone.

Backbone	VSS Block Number				Embedded Dimension
	Stage 1	Stage 2	Stage 3	Stage 4	
VMamba-Tiny	2	2	9	2	96
VMamba-Small	2	2	27	2	96
VMamba-Base	2	2	27	2	128

B Daytime and Nighttime Performance

To explore the effectiveness of our method on daytime and nighttime RGB-T images, we use the MFNet [21] dataset and follow CMX [30] to use 205 daytime images and 188 nighttime images in the test set for evaluation. As shown in Tab. B2, our method delivers better results on both daytime and nighttime results, demonstrating the effectiveness of our proposed method.

Table B2: Performance comparison on daytime and nighttime MFNet [21] dataset.

Method	Modal	Daytime mIoU (%)	Nighttime mIoU (%)
FRRN [40]	RGB	40.0	37.3
DFN [70]	RGB	38.0	42.3
BiSeNet [69]	RGB	44.8	47.7
SegFormer-B2 [59]	RGB	48.6	49.2
SegFormer-B4 [59]	RGB	49.4	52.4
MFNet [21]	RGB-T	36.1	36.8
FuseNet [22]	RGB-T	41.0	43.9
RTFNet [49]	RGB-T	45.8	54.8
FuseSeg [50]	RGB-T	47.8	54.6
GMNet [77]	RGB-T	49.0	57.7
CMX (MiT-B2) [30]	RGB-T	51.3	57.8
CMX (MiT-B4) [30]	RGB-T	52.5	59.4
Sigma (VMamba-T)	RGB-T	<u>54.1</u>	59.0
Sigma (VMamba-S)	RGB-T	55.0	<u>60.0</u>
Sigma (VMamba-B)	RGB-T	<u>54.1</u>	60.9

C Ablation Studies

Apart from the ablation studies on the effect of each of our components, we further conduct experiments on the detailed design of the State Space Models. In Tab. C3, we compare the effect of the state size in State Space Models and the number of CVSS blocks in our Mamba decoder. From the table, we can find that setting the state size to 4 and the decoder layers to [4,4,4] leads to the optimal result.

Table C3: Ablation studies of decoder layers and the space size of the state space models on the MFNet [21] dataset.

#	Encoder	State Size	Decoder Layers	mIoU (∇)
1	VMamba-T	4	[4, 4, 4]	60.5 (0.0)
2	VMamba-T	4	[3, 3, 3]	60.2 (0.3)
3	VMamba-T	4	[2, 2, 2]	59.4 (1.1)
4	VMamba-T	8	[4, 4, 4]	60.3 (0.2)
5	VMamba-T	16	[4, 4, 4]	59.7 (0.8)

D Qualitative Analysis of Different Modalities

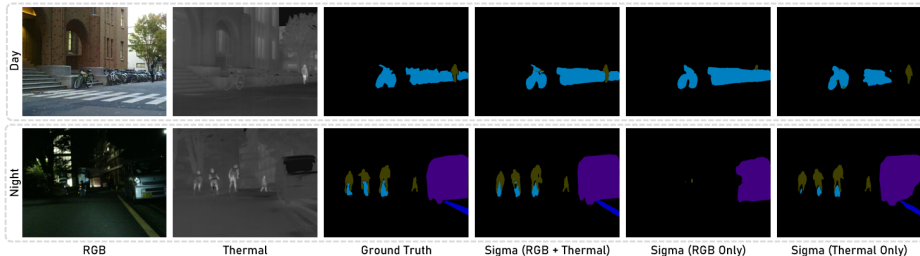


Fig. D1: Comparative analysis of semantic segmentation results: single-modal vs. multi-modal approach.

In Figure D1, we examine the contributions of both RGB and Thermal modalities to the final prediction. By leveraging information from both modalities, our Sigma model achieves more comprehensive segmentation and more precise boundary delineation, illustrating its effectiveness in extracting valuable information from both modalities.

E Complexity Comparison of CroMB and Self-Attention

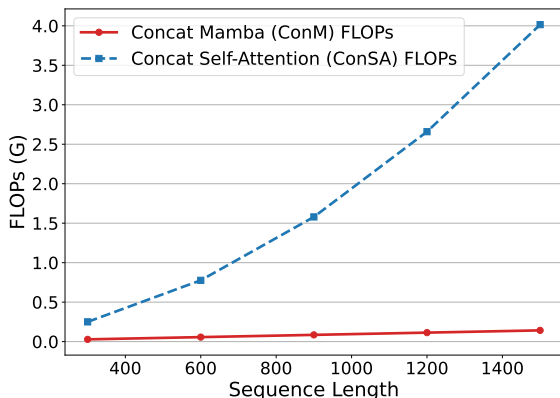


Fig. E2: Qualitative computation comparison of [Concat Self-Attention \(ConSA\)](#) and our [Concat Mamba \(ConM\)](#) mechanism.

In Fig. E2, we illustrate the qualitative growth in FLOPs as the input sequence length increases. It is evident that our ConM mechanism has much less computation consumption than constituting the State Space Model with Self-Attention. This underscores the exceptional efficiency of our proposed ConM in integrating multi-modal features.

Table E4: Quantitative comparison of computation complexity between Concat Self-Attention (ConSA) and our proposed Concat Mamba (ConM) mechanism.

Stage	Feature Size			FLOPs (G)	
	Height	Weight	Channel	ConM	ConSA
1	120	160	96	1.82	–
2	60	80	192	1.71	77.89
3	30	40	384	1.65	15.94
4	15	20	768	1.62	8.19

In Table E4, we compare the floating-point operations per second (FLOPs) of our proposed ConMB and Concat Mamba (ConSA), which employs self-attention instead of SSM. The “Stage” column indicates the four encoding stages, with the input feature size for each fusion block also provided. The findings reveal that ConMB maintains low FLOPs across all stages, whereas the FLOPs for the self-attention mechanism escalate significantly with increases in height and width.